Journal of
MATERIALS RESEARCH

A critical examination of the fundamental relations used in the analysis of nanoindentation data

Jack C. Hay
IBM Research, T. J. Watson Research Center, P.O. Box 218, Yorktown Heights, New York 10598

A. Bolshakov
Baker Hughes Inteq, P.O. Box 670968, Houston, Texas 77267-0968

G. M. Pharr[a)]
Department of Materials Science and Engineering, The University of Tennessee, 434 Dougherty Engineering Building, Knoxville, Tennessee 37996-2200 and Oak Ridge National Laboratory, Metals and Ceramics Division, P.O. Box 2008, Oak Ridge, Tennessee 37831-6116

(Received 14 September 1998; accepted 8 March 1999)

Methods for analyzing nanoindentation load-displacement data to determine hardness and elastic modulus are based on analytical solutions for the indentation of an elastic half-space by rigid axisymmetric indenters. Careful examination of Sneddon's solution for indentation by a rigid cone reveals several largely ignored features that have important implications for nanoindentation property measurement. Finite element and analytical results are presented that show corrections to Sneddon's equations are needed if accurate results are to be obtained. Without the corrections, the equations underestimate the load and contact stiffness in a manner that leads to errors in the measured hardness and modulus, with the magnitudes of the errors depending on the angle of the indenter and Poisson's ratio of the half-space. First order corrections are derived, and general implications for the interpretation of nanoindentation data are discussed.

I. INTRODUCTION

In the past two decades, a great deal of effort has been directed toward the development of techniques for characterizing the mechanical properties of thin films and small volumes of material. Load and depth sensing indentation, commonly referred to as nanoindentation, is one means by which this has been achieved.[1–12] Through the combined use of high resolution testing instrumentation and simple principles of analysis based on elastic and elastic/plastic contact theory, nanoindentation is now used routinely for small-scale mechanical property measurements, sometimes at indentation depths of only a few nanometers.[7–10]

Several analytical approaches have been developed to measure mechanical properties from indentation load-displacement data,[2–5,9–12] most of which have focused on the elastic modulus, E (Young's modulus), and the hardness, H. Central to these approaches are the methods by which experimentally measurable quantities such as the indentation load, P, the indenter penetration depth, h, and the indentation contact stiffness, $S = dP/dh$, are related to the projected contact area, A, and the elastic constants of the material, E and ν (ν = Poisson's ratio). In one form or another, most methods make use of the relation[13]

$$S = \frac{2}{\sqrt{\pi}} \frac{E}{(1 - \nu^2)} \sqrt{A} . \tag{1}$$

This fundamental equation has its roots in elastic contact theory, specifically, the analyses of Love and Sneddon for contact of an isotropic elastic half-space by rigid indenters of various geometry.[14–18] While originally derived for indentation by a rigid cone, Bulychev *et al.* showed that Eq. (1) also applies to spherical and cylindrical indenters and speculated that it may hold for other geometries as well.[19,20] Subsequently, Pharr, Oliver, and Brotzen showed that the equation applies to *any* indenter that can be described as a solid of revolution of a smooth function.[13] More recently, Cheng and Cheng have suggested that Eq. (1) is even more broadly applicable than previously thought, applying to elastic-plastic as well as purely elastic contact.[21]

The accuracy with which nanoindentation property measurements can be made is integrally tied to how well Eq. (1) models real material behavior. In this regard, it is notable that finite element studies recently have revealed what appears to be a significant shortcoming in Eq. (1) as it applies to indentation by a rigid cone.[22,23] The conical geometry is an important one because it embodies the self-similar geometry of sharp pyramidal indenters such as the Berkovich, Vickers, and cube-corner used in

[a)]Address all correspondence to this author at the University of Tennessee.

 © 1999 Materials Research Society

nanoindentation testing. In finite element simulations, the elastic and plastic properties of a material, including Young's modulus, are specified as input, and indentation load-displacement curves and contact areas are computed as output. By analyzing the output load-displacement data according to Eq. (1), it is possible to compute Young's modulus for comparison to the known input value, thus providing a check on consistency. Bolshakov and Pharr,[22] using finite element simulation to model elastic-plastic indentation by a rigid cone with a half-included angle of 70.3° (the angle that gives the same depth-to-area ratio as the Berkovich indenter), found that Young's moduli derived from Eq. (1) are consistently 5–15% too high. Ritter *et al.*,[24] Gao *et al.*,[25] and more recently Cheng and Cheng[26] have come to similar conclusions, although the magnitude of the modulus overestimation is different in each study. On the other hand, good agreement between input and derived values of E was reported by Larsen and Simo,[27] but it has been suggested that the procedure used by these investigators to determine the contact stiffness from the load-displacement data underestimated its true value, and when corrected, a modulus discrepancy even larger than that reported by Bolshakov and Pharr is observed.[28]

The observed discrepancies in finite element results led us to conduct a careful investigation of Eq. (1) as it applies to nanoindentation by conical indenters. In the course of the investigation, some largely overlooked but important subtleties in Sneddon's solution for indentation of an elastic half-space by a rigid cone were discovered that have an important bearing on the interpretation and application of the solution to nanoindentation data analysis. In-depth analysis shows that Eq. (1) and other relations commonly used in nanoindentation data reduction require modification if accurate results are to be obtained. Failure to make the modifications results in an underestimation of the load and contact stiffness in a manner that can lead to significant errors in the measurement of hardness and modulus. In this paper, the nature of the problem is documented, and approximate methods for correcting it are derived. The corrected solutions are checked for accuracy by comparison to elastic finite element simulations, and general implications for the interpretation of nanoindentation data are discussed.

II. BACKGROUND

The mathematical foundations of the problem of indentation of an elastic half-space by a rigid punch are more than a century old. In 1885, Boussinesq published a solution for the problem of contact between a solid of revolution and an elastic continuum,[29] but the solution did not lend itself to application in many problems of practical interest. Love succeeded in finding a solution for the important cases of conical[14] and cylindrical[15] punches, and later, Harding and Sneddon[16] established an analytical procedure for deriving load-displacement relations for a punch of arbitrary axisymmetric shape. A key contribution in the work of Harding and Sneddon was the realization that the problem could be reduced to solving a pair of integrals falling into a class treated by Titchmarsh[30] and Busbridge.[31] Subsequently, Sneddon showed that the method of Hankel transforms could be used to simplify the solution procedure.[17]

Figure 1(a) depicts the geometry for the special case of interest in this work, indentation by a right circular cone. A cylindrical coordinate system is chosen with radial coordinate r and axial coordinate z. The z-axis coincides with the axis of symmetry of the indenter, and the free surface of the elastic half-space defines the plane $z = 0$. The variables u and w are used to denote displacements in the r and z directions, respectively. When the indenter penetrates the half-space to a total depth, h, contact is made between the indenter and specimen along a contact depth, h_c, at which the radius of the circle of contact is a. From geometry, a and h_c are related by

$$a = h_c \tan \phi \,, \tag{2}$$

where ϕ is the half-included angle of the indenter. The boundary conditions used by Sneddon for the conical indentation problem are

$$\sigma_{zz}|_{z=0} = 0 \,, \qquad r > a \tag{3}$$

$$\sigma_{rz}|_{z=0} = 0 \,, \qquad r > 0 \tag{4}$$

$$w|_{z=0} = -h + \cot(\phi) r \,, \qquad r < a \tag{5}$$

The first condition assures that the free surface outside the radius of contact has no normal stresses acting on it, the second imposes conditions of frictionless contact, and the third forces the z-displacements of the surface to be consistent with the shape of the conical indenter.

Two important results of Sneddon's solution are the expressions for the penetration depth, h, and the indentation load, P.[16–18] The penetration depth is given by

$$h = \frac{\pi}{2} h_c = \frac{\pi a}{2 \tan \phi} \,, \tag{6}$$

which shows that the ratio of the contact depth to the total depth is constant, i.e., $h_c/h = 2/\pi$. The expression for the load is

$$P = \frac{\pi}{2} \frac{E}{(1 - \nu^2)} a h_c = \frac{2}{\pi} \frac{E}{(1 - \nu^2)} \tan \phi h^2 = \frac{\pi}{2} \frac{E}{(1 - \nu^2)} \frac{a^2}{\tan \phi} \,, \tag{7}$$

which illustrates the parabolic dependence of the load on depth, i.e., $P \sim h^2$. Combining Eqs. (6) and (7) and noting that $S = dP/dh$ and $A = \pi a^2$ yields the fundamental relation of Eq. (1).

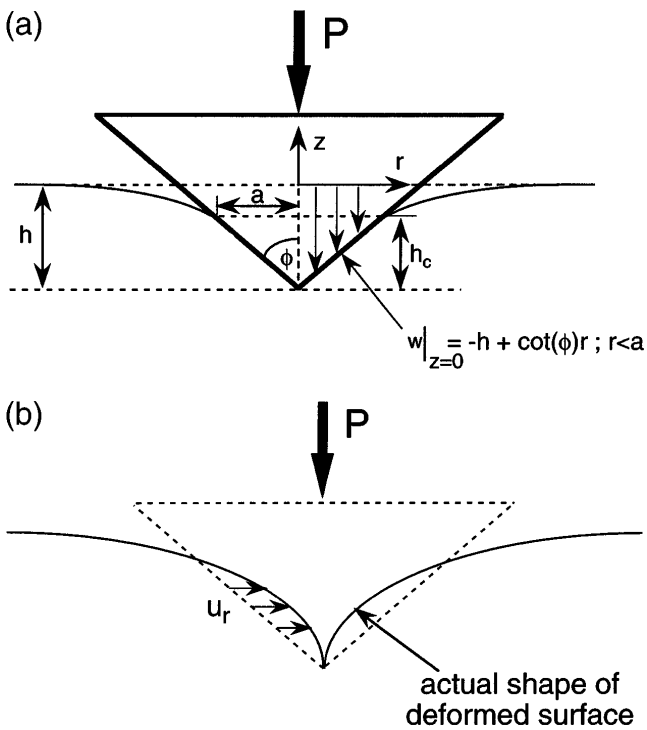

FIG. 1. (a) Geometry used by Sneddon to describe indentation of an elastic half-space by a right circular cone. (b) Schematic representation of the actual shape of the deformed surface predicted by Sneddon's analysis when the radial displacements are taken into account.

Another important result of Sneddon's analysis concerns the radial displacements of surface points inside the circle of contact. These are given by[18]

$$u = \frac{(1-2\nu)}{4(1-\nu)}\frac{r}{\tan\phi}\left[\ln\frac{r/a}{1+\sqrt{1-(r/a)^2}} - \frac{1-\sqrt{1-(r/a)^2}}{(r/a)^2}\right]. \tag{8}$$

The radial displacements, which have been overlooked in most previous studies, have an important bearing on the interpretation of Sneddon's solution for indentation by a cone. Close examination of Eq. (8) shows that the radial displacements are negative and vanish only when Poisson's ratio is 0.5 (the material is incompressible) or when the indenter angle ϕ is 90°. Thus, for most cases of practical interest ($\phi < 90°$ and $\nu < 0.5$), the radial displacements are finite. As a consequence, the shape of deformed surface inside the area of contact in the problem modeled by Sneddon is not conical, but rather a more complicated geometry like that shown schematically in Fig. 1(b).

The radial displacements in Eq. (8), in combination with the *z*-displacements imposed by the boundary condition of Eq. (5), can be used to completely describe the actual shape of the deformed surface in Sneddon's problem. Points on the originally flat surface with coordinates $r = r_0$ and $z = 0$ move to final positions given by

$$r = r_0 + u \tag{9}$$

and

$$z = -\frac{\pi a}{2\tan\phi} + \frac{r_0}{\tan\phi}, \qquad r_0 < a, \tag{10}$$

where u is defined in Eq. (8). Shifting the origin of the coordinate system to the point of maximum penetration, i.e., the tip of the indenter, the actual shape of the deformed surface is given by

$$r = z\tan\phi + \frac{(1-2\nu)}{4(1-\nu)}z\left[\ln\frac{(z\tan\phi)/a}{1+\sqrt{1-(z\tan\phi)^2/a^2}} - \frac{1-\sqrt{1-(z\tan\phi)^2/a^2}}{(z\tan\phi)^2/a^2}\right]. \tag{11}$$

Based on the predictions of Eq. (11), the deformed surface shape for indentation by a 70.3° cone is shown in Fig. 2 for three values of Poisson's ratio. Only in the case of $\nu = 0.5$ is the shape of the surface consistent with the 70.3° conical geometry; for all other Poisson's ratios, the surface is displaced inward from the 70.3° cone and is slightly curved. This means that in most cases of practical interest ($\nu < 0.5$), Sneddon's solution applies not to a perfect cone, but to a cusp-shaped indenter which approximates to a cone. It is also interesting to note that the final radial positions of points near the tip of the

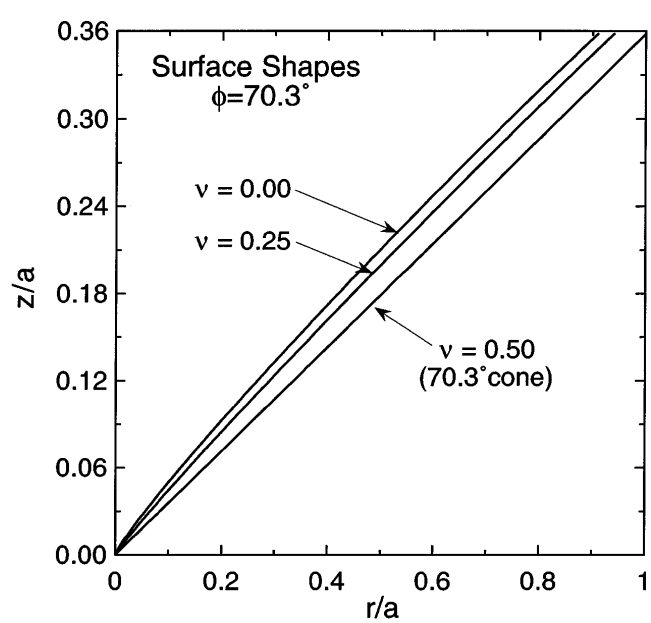

FIG. 2. The actual shape of the deformed surface in Sneddon's analysis of indentation by a rigid cone. The shapes are computed from Eq. (11) for several Poisson's ratios ($\nu = 0.0$, 0.25, and 0.5) assuming a 70.3° indenter. Only points in the region of contact are shown, i.e., from $z = 0$ to $z = h_c$.

indenter are actually *negative*, a physically meaningless situation. The implications of these observations are now examined using finite element simulation techniques.

III. FINITE ELEMENT SIMULATION

A. Procedures

To explore the consequences of the radial surface displacements, the finite element method was used to examine elastic contact by four different right-circular cones with half-included angles of 42.28°, 60°, 70.32°, and 80°. The first angle gives the same area-to-depth ratio as a cube-corner indenter, the third is that of the Berkovich and Vickers indenters, and the other two angles fill out the range of practical interest.

All calculations were carried out using the axisymmetric specimen shown in Fig. 3(a) modeled as a cylinder 103,000 nm in both length radius consisting of 2595 quadrilateral elements and 2676 nodes. To accurately simulate deformation processes in the region of contact, the mesh was refined in three stages. As illustrated in Fig. 3(b), the finest portion of the mesh was located in the region of contact near the tip of the indenter and consisted of square elements 5 nm on a side. Using an isotropic, linear-elastic, constitutive behavior characterized by Young's modulus, E, and Poisson ratio, ν, simulations proceeded in 1 nm increments of indenter displacement to a final contact depth of 50 nm using an iterative process which accounts for finite strains and rotations. A sensitivity study showed that the mesh adequately models the behavior of a semi-infinite solid.

For each indenter angle, the displacements of the nodes and the total load on the indenter were computed as a function of indenter penetration for two different sets of boundary conditions. First, to simulate exactly the problem modeled by Sneddon, the boundary conditions defined in Eqs. (3)–(5) were employed. To implement this, z-displacements consistent with the geometry of the cone were imposed on the surface nodes according to

$$z = -h + \frac{r_0}{\tan \phi}, \tag{12}$$

where r_0 is the initial radial position of the nodes in the undeformed surface ($z = 0$). However, no constraint was imposed on the radial motion of the nodes; rather, the radial displacements were determined as output of the simulation for comparison to the predictions of Sneddon's analysis [Eq. (8)]. In the second set of simulations, boundary conditions consistent with indentation by a truly rigid cone were applied. In this case, the geometry of the surface in the region of contact was forced to match that of the rigid cone subject to the condition of frictionless contact, i.e., no shear forces parallel to the interface. In all simulations, roller boundary conditions were imposed along the z-axis, as required by symmetry, and at the bottom of the specimen, where a frictionless rigid boundary was assumed [see Fig. 3(a)].

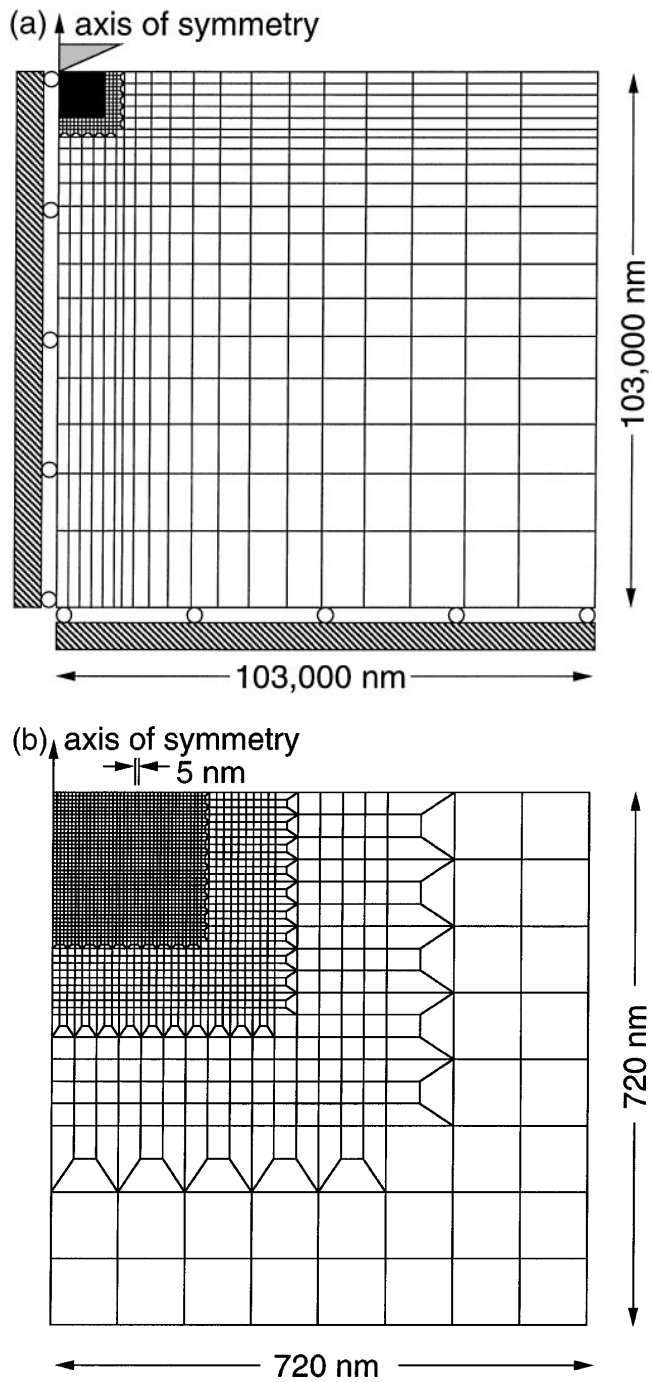

FIG. 3. The axisymmetric mesh used in finite element simulations: (a) overall mesh showing specimen dimensions and boundary conditions and (b) details of the mesh in the region of contact near the indenter tip.

B. Results

Figure 4 compares the deformed surface profiles for the two different sets of boundary conditions for a

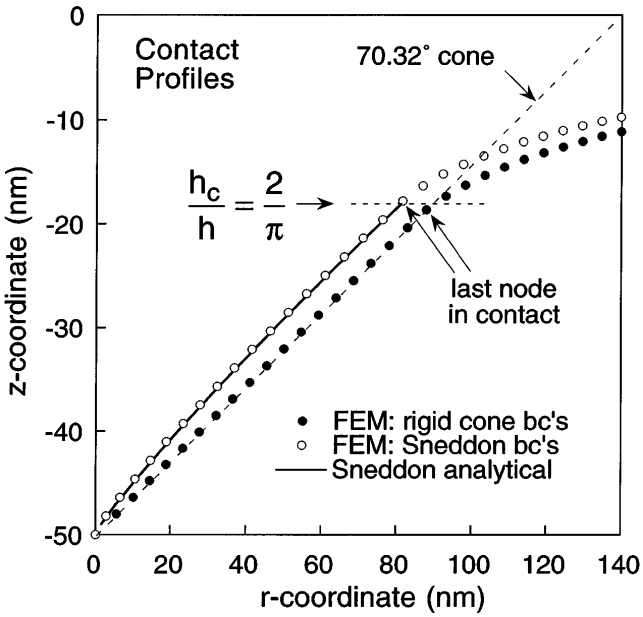

FIG. 4. Surface profiles predicted by finite element simulation for each of the two sets of boundary conditions.

material with $E = 90.85$ GPa and $\nu = 0.0$ indented by a 70.32° cone. For the purposes of illustration, a small value of Poisson's ratio is chosen since it produces the greatest difference in profile for the two sets of boundary conditions. For the rigid cone boundary conditions, the deformed surface is straight within the region of contact, coinciding perfectly with the geometry of the 70.32° cone, as it must. However, for Sneddon's boundary conditions, the surface is distinctly curved and displaced inward, thus confirming the suspected radial displacements. For comparison, the surface profile predicted by Sneddon's analytical expression for the radial displacements, Eq. (11), is also shown. Within the expected accuracy of the numerical results, the finite element and analytical predictions are essentially indistinguishable. These results thus confirm that the problem modeled by Sneddon is indeed different from that of deformation by a truly rigid cone.

Other important insight is gained by comparing the contact depth, h_c, and the contact radius, a, with Sneddon's analytical results of Eq. (6). The position of the last node in contact in the finite element simulations is shown along with the contact profiles in Fig. 4. Close inspection of the numerical results shows that for *both* sets of boundary conditions, the contact depth is related to the total penetration depth within about 1% of Sneddon's analytical prediction, $h_c = 2h/\pi$. On the other hand, Sneddon's prediction for the contact radius, $a = 2h \tan \phi/\pi$, works well only for the rigid cone; for Sneddon's exact boundary conditions, this relation overestimates the contact radius by about 9%. The overestimation is caused by the fact Eq. (6) is derived on the assumption that the deformed surface within the region of contact has the exact profile of the rigid indenter and thus inherently ignores the radial displacements. Note that a 9% overestimation of the contact radius implies a 19% overestimation of the contact area.

Figure 5 compares the simulated load-displacement curves for the two different sets of boundary conditions. Also shown in the figure are the predictions of Eq. (7), Sneddon's analytical expression for the *P-h* relationship for a conical indenter. The analytical expression matches well with the results computed using Sneddon's boundary conditions, but the loads for the rigid cone boundary conditions are about 12% larger. This is an important result, as it suggests that the analytical result of Eq. (7) does not apply to deformation by a rigid cone, but to the cusp-shaped indenter obtained when the surface radial displacements are taken into account. The larger loads also mean that the contact stiffness for indentation by a rigid cone is greater than that expected from Sneddon's analysis. Thus, the fundamental relation of Eq. (1) is also in error, a point that will be elaborated upon later.

From a physical standpoint, the larger loads required to achieve a specific displacement for the rigid cone boundary conditions can be understood in terms of the greater contact radii and greater *z*-displacements needed to further deform the curved surface of Sneddon's analysis; that is, larger loads are needed to push the curved surface outward from the cusp-shaped profile to conform with the rigid cone geometry (see Fig. 4). From this

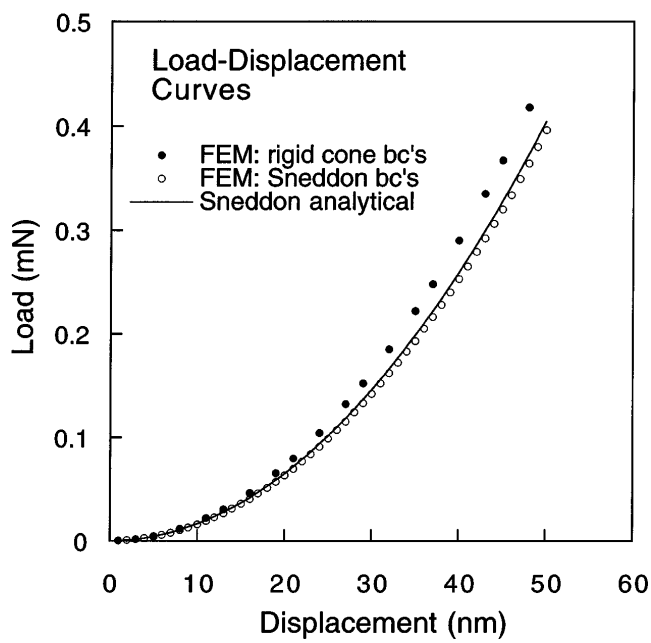

FIG. 5. Load-displacement curves predicted by finite element simulation for each of the two sets of boundary conditions.

perspective, the magnitude of the increase in load above Sneddon's prediction in Eq. (7) is expected to depend on the angle of the indenter, ϕ, and Poisson's ratio, ν, since the radial displacements depend on these parameters in the manner prescribed by Eq. (8). It is convenient to characterize the magnitude of the relative increase in load by the ratio of the load determined in the rigid cone finite element simulations to the load predicted by Sneddon's analysis evaluated from Eq. (7). This ratio, designated γ, can then be used to correct Eq. (7) to provide a more accurate description of the load-displacement relationship for deformation by a truly rigid cone. The corrected load-displacement relationship is

$$P = \gamma \frac{2}{\pi} \frac{E}{(1 - \nu^2)} \tan \phi h^2. \tag{13}$$

Values of γ determined by finite element simulation are plotted as a function of Poisson's ratio in Fig. 6. Results for four different indenters, $\phi = 42.28°$, 60°, 70.32°, and 80°, are included. Inspection of the data shows that γ decreases with increasing indenter angle and increasing Poisson's ratio and tends to unity as ν approaches 0.5 and/or ϕ approaches 90°. These observations are consistent with the notion that the radial displacements in Sneddon's problem vanish when $\nu = 0.5$ and/or $\phi = 90°$ [see Eq. (8)].

IV. MODIFICATION OF THE SOLUTION

By making a limited number of simplifying assumptions, it is possible to obtain closed-form analytical expressions for γ which can be used to modify Sneddon's solution and thereby provide a more accurate mathematical description of indentation by a rigid cone. Here, three separate methods for modifying the solution are presented. Since each is only approximate, the predictive capabilities are assessed by comparison to finite element results.

A. Contact radius matching

Perhaps the simplest approach to correcting Sneddon's solution to account for the radial displacements is shown schematically in Fig. 7. The basic idea is to apply Sneddon's results to an indenter that has a slightly larger effective cone angle, ϕ_{eff}, chosen so that when the radial displacements are taken into account, the final contact radius matches exactly that occurring by indentation with a rigid cone of angle, ϕ. As shown in the figure, this approach yields the correct contact radius and area of contact, but the profile of the deformed surface is still displaced inward from the actual desired rigid cone geometry at all points except the tip of the indenter and the contact edge. Since a larger load would be needed to displace the curved surface outward to the perfect conical geometry, this solution would appear to provide a lower bound on the indentation load. The attractiveness of this approach is that Sneddon's analytical expressions can be applied directly to the analysis, and simple closed-form solutions are easily obtained. The approach takes advantage of the observation from the finite element studies that the contact depth is a constant fraction of the total depth ($h_c/h = 2/\pi$), independent of the boundary conditions.

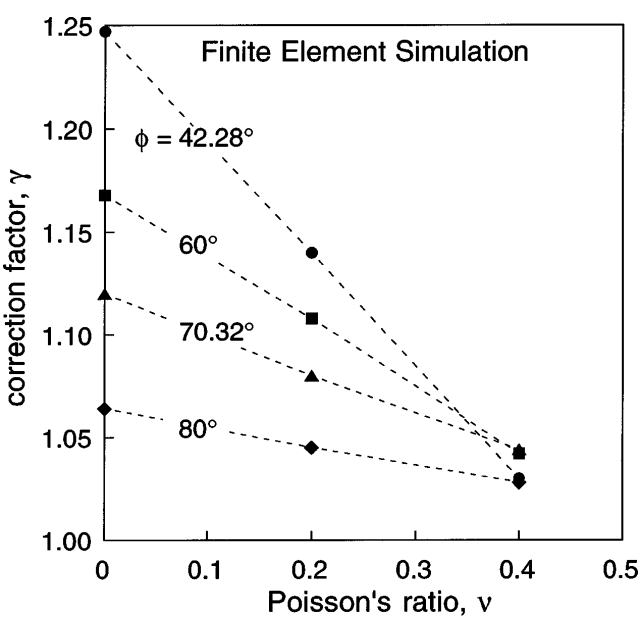

FIG. 6. Dependence of the correction factor γ on Poisson's ratio ν and the indenter angle ϕ as determined by finite element simulation.

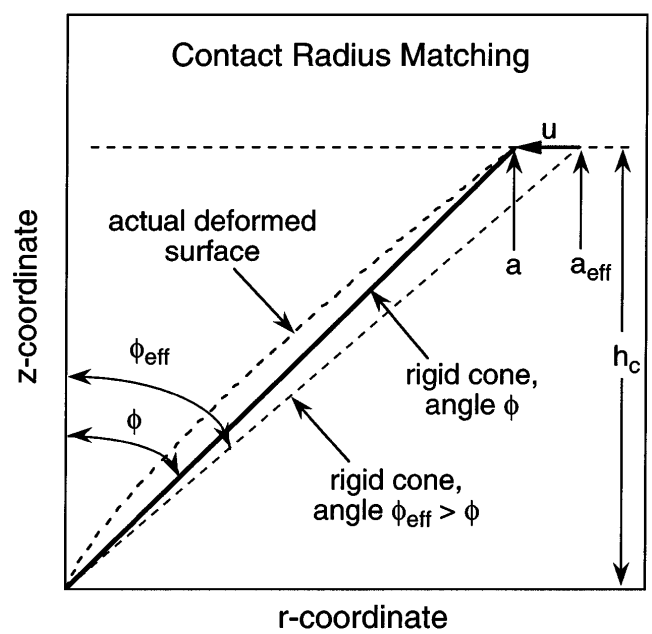

FIG. 7. Schematic representation of solution modification by contact radius matching.

The effective cone angle, ϕ_{eff}, is found by increasing the contact radius, a, by the magnitude of the anticipated radial displacement at the contact edge determined by evaluating Eq. (8) at $r = a$. This yields a contact radius for the effective indenter, a_{eff}, given by

$$a_{\text{eff}} = a\left[1 + \frac{(1 - 2\nu)}{4(1 - \nu)\tan\phi}\right], \tag{14}$$

(see Fig. 8). Since the effective cone angle is defined by

$$\tan\phi_{\text{eff}} = \frac{a_{\text{eff}}}{h_c}, \tag{15}$$

combination of Eqs. (6), (14), and (15) yields

$$\tan\phi_{\text{eff}} = \left[1 + \frac{(1 - 2\nu)}{4(1 - \nu)\tan\phi}\right]\tan\phi\,. \tag{16}$$

Replacing $\tan\phi$ in Eq. (7) by the above expression yields a modified indentation load-depth relation

$$P = \left[1 + \frac{(1 - 2\nu)}{4(1 - \nu)\tan\phi}\right]\left[\frac{2}{\pi}\frac{E}{(1 - \nu^2)}\tan\phi h^2\right], \tag{17}$$

which is precisely the form of Eq. (13) if

$$\gamma = 1 + \frac{(1 - 2\nu)}{4(1 - \nu)\tan\phi}\,. \tag{18}$$

Note that for $\nu = 0.5$ or $\phi = 90°$, $\gamma = 1$ and Sneddon's equations require no modification because there are no radial displacements. However, for all $\nu < 0.5$ and $\phi < 90°$, γ is greater than unity, and an increase in the indentation load above Sneddon's analytical result is predicted.

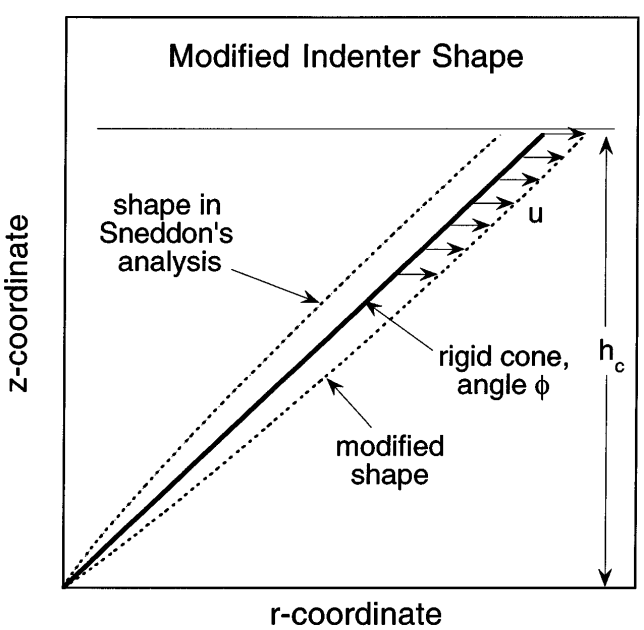

FIG. 8. Schematic representation of solution modification using a modified indenter shape.

B. Modified indenter shape

A solution that potentially provides a more accurate approximation of γ is achieved by considering an indenter whose shape deviates from the perfect conical geometry in the manner shown schematically in Fig. 8. The modified indenter is constructed by taking the perfect conical geometry and increasing the radius at each point by an amount equal to the radial displacements computed from Eq. (8). The rationale is that since the radial displacements in Sneddon's solution are negative, increasing the radius of the perfect cone at all points along the contact interface by an amount equal to the radial displacements should, to a first approximation, produce a deformed surface having a geometry close to the ideal conical shape. Using Eq. (8) to determine the magnitude of the radial displacements, the shape of the modified indenter is given by

$$r = z\tan\phi - \frac{(1 - 2\nu)}{4(1 - \nu)}z\left[\ln\frac{(z\tan\phi)/a}{1 + \sqrt{1 - (z\tan\phi)^2/a^2}} - \frac{1 - \sqrt{1 - (z\tan\phi)^2/a^2}}{(z\tan\phi)^2/a^2}\right]. \tag{19}$$

Applying Sneddon's procedures for analyzing indentation by a rigid punch of arbitrary axisymmetric profile[17] leads to a load-displacement relation exactly of the form of Eq. (13) with

$$\gamma = \pi\frac{\pi/4 + 0.15483073\cot\phi\,\frac{(1-2\nu)}{4(1-\nu)}}{\left(\pi/2 - 0.83119312\cot\phi\,\frac{(1-2\nu)}{4(1-\nu)}\right)^2}\,. \tag{20}$$

The constants appearing in this expression result from the numerical evaluation of integrals and are accurate to the number of digits shown.[32]

Following this same general approach, a slightly simpler expression for γ is obtained by assuming the curvature of the modified shape in Fig. 8 is small, in which case the indenter can be modeled as a cone of larger effective angle, ϕ_{eff}. Using linear regression to approximate the modified indenter profile of Eq. (19), methods identical to those used in the contact radius matching solution yield

$$\tan\phi_{\text{eff}} = \gamma\tan\phi\,, \tag{21}$$

where

$$\gamma = 1 + \frac{(1 - 2\nu)}{4(1 - \nu)\tan\phi}\left(3 - \frac{\pi}{2}\right). \tag{22}$$

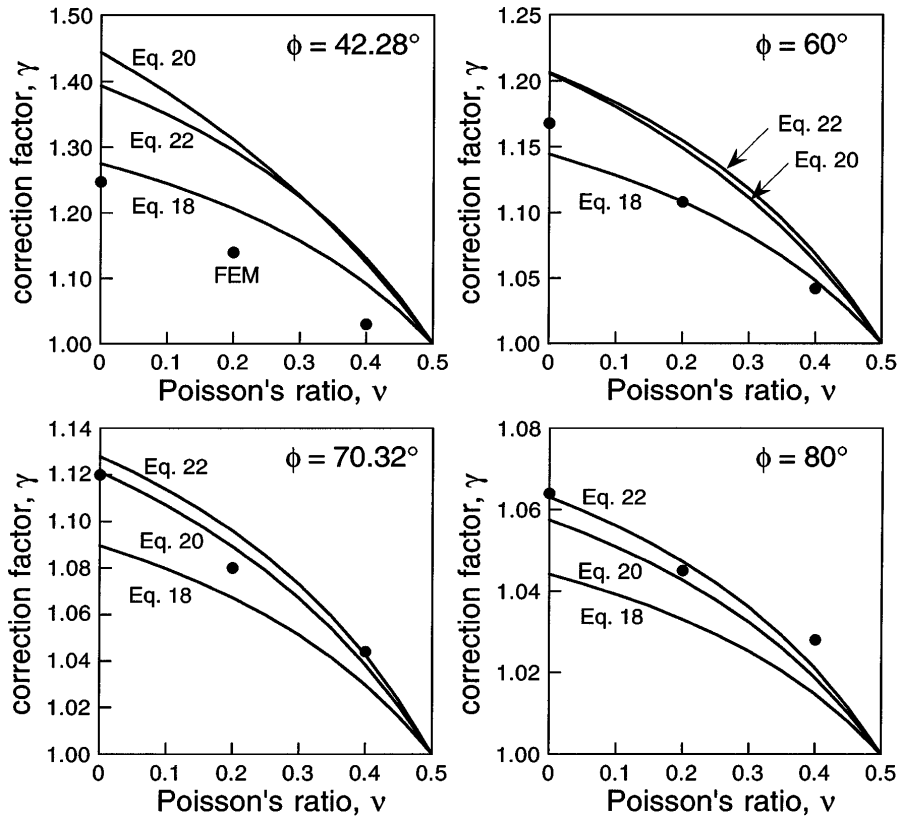

FIG. 9. Comparison of the correction factor γ evaluated from Eqs. (18), (20), and (22) with finite element simulation results.

Note that Eq. (22) is mathematically similar to Eq. (18), differing only by the factor $(3 - \pi/2)$.

C. Comparison to finite element simulations

To assess the predictive capabilities of the various analytical approximations, the dependencies of γ on ν and ϕ given by Eqs. (18), (20), and (22) are presented in Fig. 9 for comparison to the finite element results. The finite element results are shown as discrete data points at $\nu = 0$, 0.2, and 0.4. Although the general trends in the data are captured by all three equations, the expression that most accurately predicts the magnitude of γ depends on the cone angle. For the largest angle, $\phi = 80°$, Eq. (22) provides the best description, while for $\phi = 70.32°$ it is Eq. (20), and for $\phi = 60°$, Eq. (18). For the smallest cone angle, $\phi = 42.48°$, all three expressions overestimate γ, but Eq. (18) provides a reasonably close approximation. Why a given expression works well in a specific range of ϕ is not clear, but in light of these observations, it is recommended that the best approximation for γ for the two sharp indenters used most often in nanoindentation experiments, the Berkovich (equivalent cone angle = 70.32°) and cube corner (equivalent cone angle = 42.28°), are given by Eqs. (20) and (18), respectively.

V. IMPLICATIONS FOR NANOINDENTATION DATA ANALYSIS

The fact that loads larger than those predicted by Sneddon's solution are needed to describe indentation by a truly rigid cone has important implications for the analysis of nanoindentation data and the measurement of hardness and elastic modulus by nanoindentation methods. The implications are most readily seen by considering the influence of the correction factor γ on the contact stiffness, S. Since $S = dP/dh$, differentiation of Eq. (13) with respect to h in combination with the observation that $h_c/h = 2/\pi$ leads to

$$S = \gamma \frac{2}{\sqrt{\pi}} \frac{E}{(1 - \nu^2)} \sqrt{A}\,. \tag{23}$$

Comparison with Eq. (1) shows that the stiffness, like the load, is larger than predicted by Sneddon's analysis by a factor of γ. In light of this, Eq. (23) is expected to be a more accurate representation of the contact stiffness for elastic deformation by geometrically similar sharp indenters like the cone.

Exactly how this impacts nanoindentation measurements depends on the way in which the stiffness equation is used in analysis procedures. The most obvious is in the measurement of elastic modulus from experimentally

determined contact stiffnesses and contact areas. Such measurements frequently are made using Eq. (23) in the form

$$E = \frac{1}{\gamma}\frac{\sqrt{\pi}}{2}\frac{S}{\sqrt{A}}(1 - \nu^2), \tag{24}$$

with $\gamma = 1$. However, since $\gamma > 1$, failure to include the correction factor in the analysis leads to an overestimation of E, the extent of which depends on the cone angle of the indenter and Poisson's ratio of the specimen in the manner approximated by Eqs. (18), (20), and (22).

It is instructive to consider how large the overestimations of elastic modulus may be in typical experimental situations. Using Eq. (20) to provide a value of γ for use with a Berkovich indenter (equivalent cone angle = 70.32°), the elastic modulus of a material with Poisson's ratio $\nu = 0.25$ is overestimated by about 8% if γ is taken to be unity. This is the origin of the 5–15% discrepancy between moduli input into finite element simulations and those derived from the load-displacement output.[22,23] Note that the modulus overestimation is even larger for smaller indenter angles; for the cube corner indenter (equivalent cone angle = 42.28°), for which Eq. (18) gives the best description of γ, the overestimation of E is about 18% when it is assumed that $\gamma = 1$.

A less obvious but equally important impact concerns the determination of indenter shape functions (or area functions).[9] In one common procedure, shape functions are determined using Eq. (23) rewritten as:

$$A = \frac{1}{\gamma^2}\frac{\pi}{4}\left[\frac{S(1 - \nu^2)}{E}\right]^2. \tag{25}$$

By performing experiments in a calibration material of known modulus (fused quartz is frequently used), Eq. (25) can be used in conjunction with experimental measurements of the contact stiffness to deduce the contact area as a function of depth, from which the shape function is derived. Note, however, that if the correction factor γ is ignored, i.e., $\gamma = 1$ as in Eq. (1), the areas deduced from this procedure are too large by a factor of γ^2. Using Eqs. (20) and (18) to estimate γ for indentation in fused quartz ($\nu = 0.17$), failure to account for the factor $1/\gamma^2$ in Eq. (25) leads to an overestimation of the shape function area by 20% for the Berkovich indenter and 49% for the cube corner indenter. Since the hardness depends inversely on the area deduced from the shape function through $H = P/A$, the shape function error will result in an error of similar magnitude in the hardness. Curiously, however, the modulus measured using the incorrect shape is not necessarily subject to the same error. This is because when areas too large by a factor of γ^2 are used to compute the modulus by means of Eq. (1), the net effect is to reduce the calculated modulus by a factor of $1/\gamma$, exactly as prescribed in Eq. (24). Errors will occur in the modulus measurement only if Poisson's ratio for the material differs from that used in the shape function calibration material. If the two Poisson's ratios are the same, the measurement procedure gives the correct value for the modulus, even though the shape function is wrong.

Lastly, two words of caution are in order with respect to the application of these observations to nanoindentation measurements. The first caution stems from the fact that the relations derived in this work formally apply only to indentation of an *elastic* half-space. For the more realistic case of *elastic-plastic* deformation, the situation is considerably more complex and difficult to analyze. In this regard, it is noteworthy that finite element simulations of conical indentation of elastic-plastic materials have shown that problems similar to those identified here are also observed in elastic-plastic materials.[22] In fact, the finite element results show that for very plastic materials, as characterized by large values of the modulus-to-yield strength ratio, E/σ_y, even larger values of γ may be needed to obtain accurate measurements of E.[22] The second caution relates to the fact that the relations derived here apply to deformation by a *rigid* cone; i.e., elasticity in the indenter is not considered. While this assumption is reasonable when the modulus of the indenter is much greater than that of the specimen, as is often the case when diamond indenters are employed, it is probably not so reasonable when the modulus of the indenter and the specimen are similar, as would be the case when testing diamond or diamond films. Further examination of these issues is currently underway.

VI. CONCLUSIONS

When the radial surface displacements in Sneddon's solution for penetration of an elastic half-space by a conical indenter are taken into account, the shape of the deformed surface is subtly curved in a manner that is not consistent with deformation by a rigid cone. Finite element simulations show that indentation by a rigid cone requires larger loads than those predicted by Sneddon's analysis. As a consequence, the fundamental relation between contact stiffness, elastic modulus, and contact area used frequently in nanoindentation measurements requires modification to the form

$$S = \gamma\frac{2}{\sqrt{\pi}}\frac{E}{(1 - \nu^2)}\sqrt{A},$$

where γ is a correction factor that depends on the half-included angle of the indenter, ϕ, and Poisson's ratio, ν, of the indented material. Analytical approximations for γ derived by applying simple modifications to Sneddon's

solution yield:

$$\gamma = \pi \frac{\pi/4 + 0.15483073 \cot \phi \frac{(1-2\nu)}{4(1-\nu)}}{\left(\pi/2 = 0.83119312 \cot \phi \frac{(1-2\nu)}{4(1-\nu)}\right)^2}$$

(Berkovich indenter; $\phi = 70.32°$)

and

$$\gamma = 1 + \frac{(1 - 2\nu)}{4(1 - \nu) \tan \phi}$$

(cube-corner indenter; $\phi = 42.28°$)

for the Berkovich and cube-corner indenters used frequently in nanoindentation experiments. These values for γ can be used to provide more accurate measurements of hardness and elastic modulus from nanoindentation load-displacement data.

ACKNOWLEDGMENTS

This research was sponsored by the Division of Materials Sciences, United States Department of Energy, under contract DE-AC05-96OR22464 with Lockheed Martin Energy Research Corp., through the SHaRE Program under Contract DE-AC05-76OR00033 with Oak Ridge Associated Universities, and by an appointment (JCH) to the ORNL Postdoctoral Research Associates Program administered jointly by the Oak Ridge Institute for Science and Education and ORNL.

REFERENCES

1. D. Newey, M. A. Wilkins, and H. M. Pollock, J. Phys. E: Sci. Instrum. **15**, 119–122 (1982).
2. S. I. Bulychev, V. P. Alekhin, M. Kh. Shorshorov, A. P. Ternovskii, and G. D. Shnyrev, Zavod. Lab. **41**, 1137 (1975).
3. M. Kh. Shorshorov, S. I. Bulychev, and V. P. Alekhin, Sov. Phys. Dokl. **26**, 769 (1981).
4. S. I. Bulychev and V. P. Alekhin, Zavod. Lab. **53**, 76 (1987).
5. J. L. Loubet, J. M. Georges, O. Marchesini, and G. Meille, J. Tribology **106**, 43 (1984).
6. F. Frolich, P. Grau, and W. Grellmann, Phys. Status Solidi **42**, 79 (1977).
7. J. B. Pethica, R. Hutchings, and W. C. Oliver, Philos. Mag. A **48**, 593 (1983).
8. D. Stone, W. R. LaFontaine, P. Alexopoulos, T-W. Wu, and C-Y. Li, J. Mater. Res. **3**, 141 (1988).
9. W. C. Oliver and G. M. Pharr, J. Mater. Res. **7**, 1564 (1992).
10. M. F. Doerner and W. D. Nix, J. Mater. Res. **1**, 601 (1986).
11. J. S. Field and M. V. Swain, J. Mater. Res. **8**, 297 (1993).
12. J. S. Field and M. V. Swain, J. Mater. Res. **10**, 101 (1995).
13. G. M. Pharr, W. C. Oliver, and F. R. Brotzen, J. Mater. Res. **7**, 613 (1992).
14. A. E. H. Love, Quart. J. Math. **10**, 161 (1939).
15. A. E. H. Love, Philos. Trans. A **228**, 377 (1929).
16. J. W. Harding and I. N. Sneddon, *Proc. Cambridge Philos. Soc.* **41**, 16 (1945).
17. I. N. Sneddon, Int. J. Eng. Sci. **3**, 47 (1965).
18. I. N. Sneddon, *Fourier Transforms* (McGraw-Hill Book Company, Inc., New York, 1951), pp. 450–467.
19. S. I. Bulychev, V. P. Alekhin, M. Kh. Shorshorov, A. P. Ternovskii, and G. D. Shnyrev, Zavod. Lab. **41**, 1137 (1975).
20. S. I. Bulychev, V. P. Alekhin, M. Kh. Shorshorov, and A. P. Ternovskii, Prob. Prochn. **9**, 79 (1976).
21. C-M. Cheng and Y-T. Cheng, Appl. Phys. Lett. **71**, 2623 (1997).
22. A. Bolshakov and G. M. Pharr, J. Mater. Res. **13**, 1049 (1998).
23. A. Bolshakov, W. C. Oliver, and G. M. Pharr, in *Thin Films: Stresses and Mechanical Properties VI*, edited by W. W. Gerberich, H. Gao, J-E. Sundgren, and S. P. Baker (Mater. Res. Soc. Symp. Proc. **436**, Pittsburgh, PA, 1997), p. 141.
24. J. E. Ritter, T. J. Lardner, D. T. Madsen, and R. J. Gionazzo, in *Materials in Microelectronic and Optoelectronic Packaging* (The American Ceramic Society, Westerville, OH), p. 379.
25. H. Gao, C-H. Chiu, and J. Lee, Int. J. Solids Struct. **29**, 2471 (1992).
26. Y-T. Cheng and C-M. Cheng, J. Appl. Phys. **84**, 1284 (1998).
27. T. A. Larsen and J. C. Simo, J. Mater. Res. **7**, 618 (1992).
28. A. Bolshakov and G. M. Pharr, in *Thin Films: Stresses and Mechanical Properties VI*, edited by W. W. Gerberich, H. Gao, J-E. Sundgren, and S. P. Baker (Mater. Res. Soc. Symp. Proc. **436**, Pittsburgh, PA, 1997), p. 189.
29. J. Boussinesq, *Applications des Potentiels a l'etude de equilibre dt du mouvement des solides elastiques* (Gauthier-Villars, Paris, 1885).
30. E. C. Titchmarsh, *Introduction to the Theory of Fourier Integrals* (Clarendon Press, Oxford, 1937).
31. I. W. Busbridge, Proc. London Math. Soc. **44**, 115 (1938).
32. A. Bolshakov, Ph.D. Thesis, Rice University, 1996.